Lithium Fluoride Embedded Prelithiated Graphite Interface Layer Enables Stable All-solid-state Lithium Ion Batteries

Nini Zhang,[a, b] Dingcheng Guo,[a] Qili Su,[c] Shungui Deng,[a] Yong Lu,[c] Zhe Li,*[c] Haijing Liu,*[c] and Xiayin Yao*[a, b]

All-solid-state rechargeable batteries are regarded as one of the most promising next-generation energy storage devices, while their cycling stability is still a great challenge due to the nonuniform lithium ion transportation and the loss of active lithium during cycling. Herein, a LiF embedded prelithiated graphite interface layer is designed and inserted between Li_6PS_5Cl solid electrolyte layer and graphite anode layer. The presence of LiF, C—F bonds and prelithiated graphite in this unique interface layer can facilitate uniform lithium ion migration and compensate the loss of active lithium, thus significantly improving the cyclic performances of both monop-

olar and bipolar all-solid-state lithium ion batteries. After 100 cycles at 0.1 C, the capacity retention increases from 58% to 78.5% for the monopolar $LiNi_{0.5}Co_{0.2}Mn_{0.3}O_2|Li_6PS_5Cl|LiF@2.5\%$ Li@G|graphite all-solid-state lithium ion battery. Besides, the bipolar all-solid-state lithium ion batteries show a high discharge plateau of ~7.6 V with a capacity retention of 60.2% after 190 cycles at 0.1 C. This work demonstrates the effectiveness of LiF embedded prelithiated graphite interface layer for improving the electrochemical performances of all-solid-state lithium ion batteries.

1. Introduction

Benefiting from the great potential in improved energy density and safety, all-solid-state batteries have gained considerable recognition as the next generation energy storage technology.[1–2] As an important part of all-solid-state batteries, solid electrolytes, especially the sulfide-based solid electrolytes, are favored for higher ionic conductivity compared with those of the oxide- and polymer-based counterparts.[3] Among various sulfide solid electrolytes, argyrodite structured Li_6PS_5Cl has received much attention for all-solid-state lithium rechargeable batteries due to high ionic conductivity, good electrochemical stability and excellent ductility.[4–5] However, the uncontrollable parasitic interfacial reactions between Li_6PS_5Cl and lithium metal as well as lithium dendrites growth greatly deteriorate the battery cyclic performances and lead to potential internal short circuits in the batteries.[6–7]

To improve interface compatibility of sulfide solid electrolytes and lithium metal anode, different strategies have been developed, such as manipulating solid electrolytes with differ-

ent dopants, inserting an artificial interlayer between sulfide solid electrolytes and lithium metal anode, and employing three-dimensional structure lithium metal anode.[6,8–12] Combined with the favorable thermodynamic stability and high lithium interfacial energy, LiF is an essential component in stabilizing the solid electrolyte interphase layer and inhibiting dendrite formation.[13–14] Liu et al. reported the fluorinated $Li_{6.3}P_{0.9}Mg_{0.1}S_5Cl_{0.8}F_{0.2}$ with Mg and F co-doping.[15] The introduction of F generates a robust LiF-containing interface between the electrolyte and lithium metal anode, which effectively prevents the decomposition of sulfide solid electrolytes and suppresses the growth of lithium dendrites onto or inside the sulfide solid electrolytes. Different from using fluorine doped sulfide solid electrolytes to induce the formation of functional solid electrolyte interphase layer with high concentration of LiF, Shen et al. in situ constructed a LiF-rich multifunctional interface on the surface of lithium metal by spontaneous reaction between lithium metal and poly(tetrafluoroethylene) (PTFE) at room temperature.[16] The highly fluorinated interface significantly facilitates the diffusion of lithium ions within the solid electrolyte interface layer and avoids the generation of lithium dendrites. Clearly, the lithium fluoride-containing solid electrolyte interphase layer could well stabilize the interface for all-solid-state lithium batteries.

Unlike lithium metal anode, graphite anode generally exhibits excellent cyclability with small volume change in all-solid-state lithium ion batteries.[17–18] However, similar to the lithium metal anode, lithium deposition on graphite anode surface would form lithium dendrites during the charge process.[19–20] Due to their inherent reactivity nature, the unstable deposited lithium presents high reactivity with the solid electrolytes, gradually forming a unstable interfaces.[21] Besides, during lithiation process, the formation of solid electrolyte interface film and its proliferation process will consume

[a] N. Zhang, D. Guo, S. Deng, Prof. Dr. X. Y. Yao
Ningbo Institute of Materials Technology and Engineering, Chinese Academy of Sciences, Ningbo 315201, P. R. China
E-mail: yaoxy@nimte.ac.cn

[b] N. Zhang, Prof. Dr. X. Y. Yao
Center of Materials Science and Optoelectronics Engineering, University of Chinese Academy of Sciences, Beijing 100049, P. R. China

[c] Dr. Q. Su, Dr. Y. Lu, Dr. Z. Li, Dr. H. J. Liu
China Science Lab, General Motors Global Research & Development, Shanghai 201206, P. R. China
E-mail: zhe.4.li@gm.com
        helen.liu@gm.com

🖥 Supporting information for this article is available on the WWW under https://doi.org/10.1002/batt.202300488

active lithium, resulting in a decrease in the overall capacity and an increase in internal resistance.[22–23] Adding extra active lithium to compensate for the loss of active lithium in graphite anode is an effective way to address this issue, including physical lithium replenishment based on metal lithium, chemical lithium replenishment, electrochemical lithium replenishment etc.[24–25] Nevertheless, it is still difficult to directly use lithium powder to graphite anode due to its thermodynamic instability with the sulfide solid electrolytes.

Considering these challenges, we proposed a LiF embedded prelithiated graphite interface layer by spontaneous reaction among lithium metal powder, graphite and PTFE. After uniformly distributing lithium powder into graphite, a prelithiated graphite generated, and the residual unreacted lithium would further react with the addition of PTFE. Thus, a 6 μm-thick LiF-embedded prelithiated graphite layer composed of LiF, C−F bonds and prelithiated graphite is realized and inserted between Li_6PS_5Cl solid electrolyte and graphite anode, which not only compensates the irreversible lithium loss of graphite anode but also avoids the direct contact between lithium and solid electrolyte. Meanwhile, the formation of high fluorine-containing interface is conducive to impeding the growth of lithium dendrites into solid electrolytes and avoiding short-circuit during charge/discharge process, resulting in significantly improved cycling stability in both monopolar and bipolar all-solid-state lithium ion batteries.

2. Results and Discussion

The synthesis route for LiF-embedded prelithiated graphite in all-solid-state lithium batteries is presented in Figure 1. Graphite was first mixed with a certain amount lithium powder, which was transferred to an aluminum plastic bag and pressed at 10 MPa. After keeping at 100 °C for 6 hours, lithium powder would spontaneously react with graphite and thus generates prelithiated graphite, which were labeled as 0.5 %Li@G, 1.0 % Li@G, 2.5 %Li@G and 5 %Li@G with different amount of lithium powder of 0.5 wt %, 1.0 wt %, 2.5 wt % and 5.0 wt %, respectively (Figure S1). With increasing the lithium contents, the degree of lithiation increases. The intercalation of lithium ions into the graphite layers enlarges the graphite layer spacing as confirmed by the peak shifting to lower angles in the X-ray diffraction (XRD) patterns (Figure 2a).

The resultant prelithiated graphite were further mixed with 1 wt % PTFE for 1 hour and then standing for 6 hours. PTFE is easy defluorinated with lithium metal and transferred to LiF and amorphous carbon, resulting in LiF-embedded prelithiated graphite, denoted as LiF@0.5 %Li@G, LiF@1.0 %Li@G, LiF@2.5 % Li@G and LiF@5.0 %Li@G with different prelithiated graphite samples. To demonstrate the chemical compositions of LiF-embedded prelithiated graphite, X-ray photoelectron spectroscopy (XPS) was conducted with LiF@2.5 %Li@G. Figure 2c displays the XPS F 1s profiles, obvious peak at 684.7 eV and 686.5 eV are observed, confirming the existence of LiF, which could promote lithium ion migration along the interface and prevent lithium dendrite growth due to its low electronic conductivity and high interfacial energy. Besides, the C−F bonds at 290.6 eV are also observed, indicating defluorination of PTFE is incomplete. The C−F bonds have been demonstrated to form homogenous lithium ion flux and facilitate lithium migration.[16] In addition, once lithium dendrite forms, it will be consumed by the remaining C−F bonds and then converted into LiF. The as-synthesized LiF-embedded prelithiated graphite is employed as interface layer between solid electrolyte layer and graphite anode layer, as depicted in Figure 1.
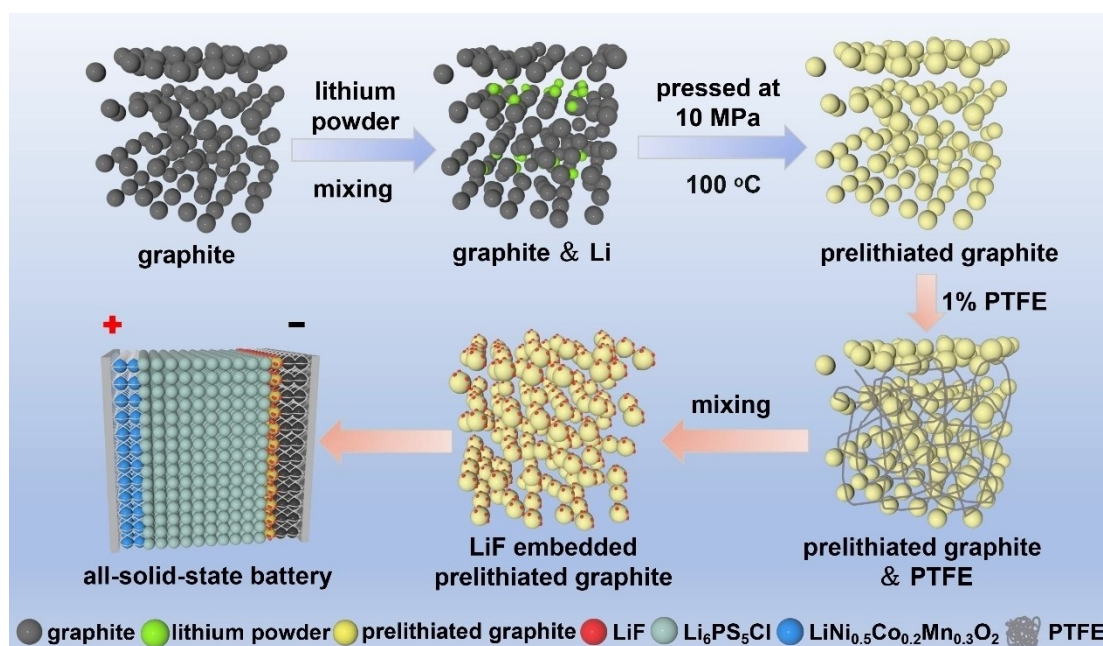

Figure 1. Schematic of the synthesis route for LiF-embedded prelithiated graphite in all-solid-state lithium ion batteries.

Batteries & Supercaps

Research Article
doi.org/10.1002/batt.202300488

Chemistry
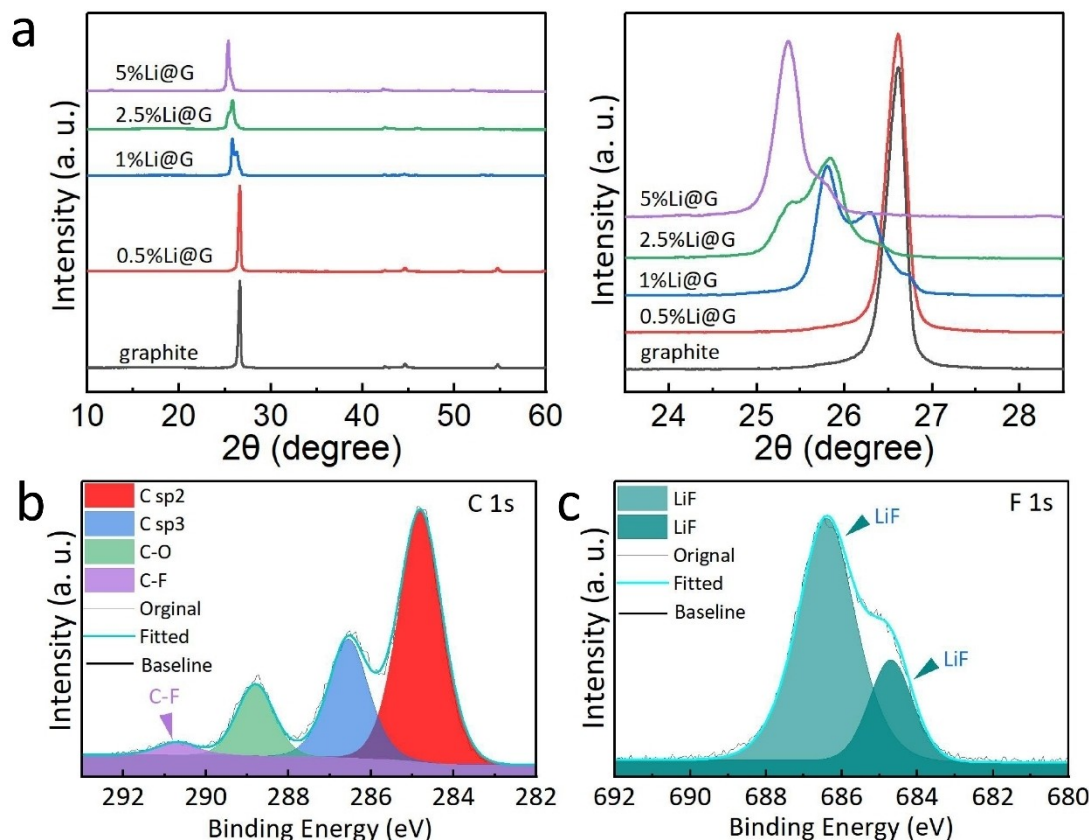Europe

European Chemical
Societies Publishing

Figure 2. (a) XRD patterns of prelithiated graphite and magnified view of the main diffraction peak. (b) High-resolution XPS C 1s and (C) F 1s of LiF@2.5%Li@G.

As shown in Figure 3, the electrochemical performances of $LiNi_{0.5}Co_{0.2}Mn_{0.3}O_2|Li_6PS_5Cl|graphite$ all-solid-state lithium ion batteries based on dry-film electrodes were evaluated. Figure 3a presents the XRD pattern of graphite anode dry film and reveals that graphite and Li_6PS_5Cl solid electrolyte are the main components. Figure 3b displays a digital photograph of a graphite dry film with a diameter of 10 mm. SEM and energy-dispersive X-ray spectroscopy (EDS) analyses demonstrate that various elements are uniformly distributed throughout the graphite dry film (Figure 3c and 3d). The detailed information of individual element distribution is also shown in Figure S2, clearly demonstrating the homogenous distribution of each component. Figure 3e illustrates the XRD pattern of $LiNi_{0.5}Co_{0.2}Mn_{0.3}O_2$ cathode dry film and all diffraction peaks can be assigned to $LiNi_{0.5}Co_{0.2}Mn_{0.3}O_2$ and Li_6PS_5Cl solid electrolyte. Figure 3f provides a digital photograph of an intact 10 mm diameter $LiNi_{0.5}Co_{0.2}Mn_{0.3}O_2$ dry film. SEM and EDS analyses confirm the even distribution of various elements in the $LiNi_{0.5}Co_{0.2}Mn_{0.3}O_2$ dry film (Figure 3g and 3h, Figure S3). The electrochemical performances of all-solid-state lithium batteries using graphite or $LiNi_{0.5}Co_{0.2}Mn_{0.3}O_2$ as working electrode and Li–In as counter electrode were tested. The initial discharge/charge curves of graphite and $LiNi_{0.5}Co_{0.2}Mn_{0.3}O_2$ dry film based cells are depicted in Figure S4, showing reversible capacities of 352.7 mAh g^{-1} and 161.1 mAh g^{-1} for graphite and $LiNi_{0.5}Co_{0.2}Mn_{0.3}O_2$, respectively. However, with N/P ratio of 1.1, the $LiNi_{0.5}Co_{0.2}Mn_{0.3}O_2|Li_6PS_5Cl|graphite$ all-solid-state lithium

ion battery only delivers a reversible capacity of 123.8 mAh g^{-1}, much lower than that of $LiNi_{0.5}Co_{0.2}Mn_{0.3}O_2|Li_6PS_5Cl|Li–In$ cell. With increasing N/P ratios ranging from 1.1 to 1.5, a satisfactory maximum reversible capacity of 150.7 mAh g^{-1} can be obtained with a N/P ratio of 1.4 (Figure 3i). Furthermore, the assembly pressure is an important factor affecting its performances. Thus, $LiNi_{0.5}Co_{0.2}Mn_{0.3}O_2|Li_6PS_5Cl|graphite$ all-solid-state lithium ion batteries based on dry-film electrodes under different assembly pressures were assembled by applying different pressures to the prototype cell using a hydraulic press. The cyclic performances are shown in Figure 3j and Figure S5, rapid capacity decay is observed under a low assemble pressure of 90 MPa. Increasing the assembly pressure to 270 MPa, the cell exhibits enhanced cycling stability.

In order to further improve the cyclic performances of $LiNi_{0.5}Co_{0.2}Mn_{0.3}O_2|Li_6PS_5Cl|graphite$ all-solid-state lithium ion batteries with N/P ratio of 1.4 under 270 MPa, a 6 μm-thick LiF@2.5%Li@G interface layer was inserted between Li_6PS_5Cl solid electrolyte and graphite anode. The cross-sectional SEM image of the cell is shown 4a and the corresponding EDS mappings of S, P, and Cl elements indicate that LiF@2.5%Li@G interface layer is seamlessly connected to both the graphite anode and Li_6PS_5Cl electrolyte (Figure 4b–d). And the $LiNi_{0.5}Co_{0.2}Mn_{0.3}O_2|Li_6PS_5Cl|graphite$ cell also exhibits integrate solid electrolyte/anode interface (Figure S6). As shown in Figure 4e, the $LiNi_{0.5}Co_{0.2}Mn_{0.3}O_2|Li_6PS_5Cl|graphite$ all-solid-state lithium ion battery delivers an initial discharge capacity of

Batteries & Supercaps

Research Article
doi.org/10.1002/batt.202300488

Chemistry Europe
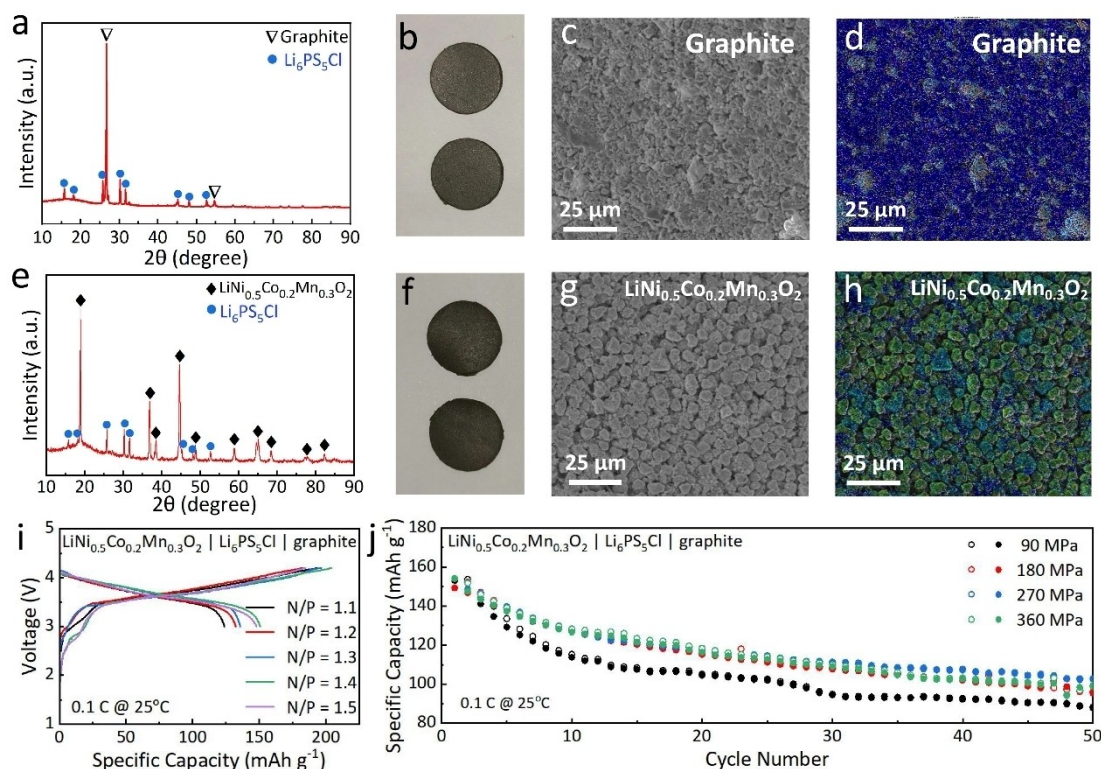European Chemical
Societies Publishing

Figure 3. (a) XRD pattern, (b) optical photograph, (c) SEM image and corresponding (d) EDS image of graphite dry film. (e) XRD pattern, (f) optical photograph, (g) SEM image and corresponding (h) EDS image of $LiNi_{0.5}Co_{0.2}Mn_{0.3}O_2$ dry film. (i) The discharge/charge profiles of $LiNi_{0.5}Co_{0.2}Mn_{0.3}O_2|Li_6PS_5Cl|$graphite all-solid-state lithium ion batteries by dry-film approach under different N/P ratios. (j) The cyclic performances of $LiNi_{0.5}Co_{0.2}Mn_{0.3}O_2|Li_6PS_5Cl|$graphite all-solid-state lithium ion batteries by dry-film approach under different assembly pressures.

154.1 mAh g^{-1} with a capacity retention of 58% after 100 cycles. Coupling with LiF@2.5%Li@G interface layer, both discharge plateau and initial capacity of the $LiNi_{0.5}Co_{0.2}Mn_{0.3}O_2|Li_6PS_5Cl|$ LiF@2.5%Li@G|graphite all-solid-state lithium ion battery are almost changeless, while the capacity retention increases to 78.5% after 100 cycles. Actually, the lithium amount in LiF-embedded prelithiated graphite interface layer also affect the cycling stability and $LiNi_{0.5}Co_{0.2}Mn_{0.3}O_2|Li_6PS_5Cl|$LiF@2.5%Li@G| graphite possesses the best cyclic performances (Figure S7 and Figure S8). The lithium ion migration schematic diagram across the interface layer is shown in Figure 4h. Without LiF@2.5% Li@G interface layer, lithium ions transport from $LiNi_{0.5}Co_{0.2}Mn_{0.3}O_2$ cathode side to graphite anode and intercalate into the graphite layer randomly accompanied by side reactions, causing the loss of active lithium and reducing the coulombic efficiency of the battery. Nevertheless, for $LiNi_{0.5}Co_{0.2}Mn_{0.3}O_2|Li_6PS_5Cl|$LiF@2.5%Li@G|graphite cell, the presence of LiF and C—F bonds could prevent interface side reactions, uniform lithium ion flux, facilitate lithium ion migration and suppress lithium dendrite growth. Also, more active lithium is provided to compensate for the loss of active lithium in the side reactions, thus significantly enhancing the cycling stability.

The rate performances were further tested under the current densities ranging from 0.1 C to 0.5 C, as shown in Figure 5a. The $LiNi_{0.5}Co_{0.2}Mn_{0.3}O_2|Li_6PS_5Cl|$LiF@2.5%Li@G| graphite all-solid-state lithium ion battery delivers 149.8, 130.7,

121.8, 107.8, and 98.6 mAh g^{-1} at 0.1, 0.2, 0.3, 0.4, and 0.5 C, respectively. And when the current turns back to 0.1 C, a high capacity of 141.9 mAh g^{-1} can be recovered. By contrast, reversible capacities of only 146.4, 120.4, 103.7, 85, and 71 mAh g^{-1} at 0.1, 0.2, 0.3, 0.4, and 0.5 C are observed for $LiNi_{0.5}Co_{0.2}Mn_{0.3}O_2|Li_6PS_5Cl|$graphite all-solid-state lithium ion battery, which recovers to 129 mAh g^{-1} when the current density is reset to 0.1 C. In addition, the effectiveness of LiF@2.5%Li@G interface layer is demonstrated in bipolar all-solid-state lithium ion batteries (Figure S9). Figures 5b and 5c show discharge/charge profiles of the bipolar all-solid-state lithium ion batteries, exhibiting a high discharge plateau of ~7.6 V. The $LiNi_{0.5}Co_{0.2}Mn_{0.3}O_2|Li_6PS_5Cl|$LiF@2.5%Li@G|graphite all-solid-state bipolar lithium ion battery delivers a slightly higher initial discharge capacity of 158.6 mAh g^{-1} than that of $LiNi_{0.5}Co_{0.2}Mn_{0.3}O_2|Li_6PS_5Cl|$graphite bipolar cell with 154 mAh g^{-1}. After 190 cycles, a reversible capacity of 95.5 mAh g^{-1} can be maintained with capacity retention of 60.2% for $LiNi_{0.5}Co_{0.2}Mn_{0.3}O_2|Li_6PS_5Cl|$LiF@2.5%Li@G|graphite bipolar cell. In sharp contrast, $LiNi_{0.5}Co_{0.2}Mn_{0.3}O_2|Li_6PS_5Cl|$graphite all-solid-state bipolar cell only shows 57 mAh g^{-1} with a capacity retention of 37% after 190 cycles. Clearly, with the assistance of LiF@2.5%Li@G interface layer, the all-solid-state lithium ion batteries based on $LiNi_{0.5}Co_{0.2}Mn_{0.3}O_2$ cathode and graphite anode show significantly enhanced cycling stability and rate capability in monopolar cell. Most importantly, the cyclic performance of bipolar cell is also substantially improved.
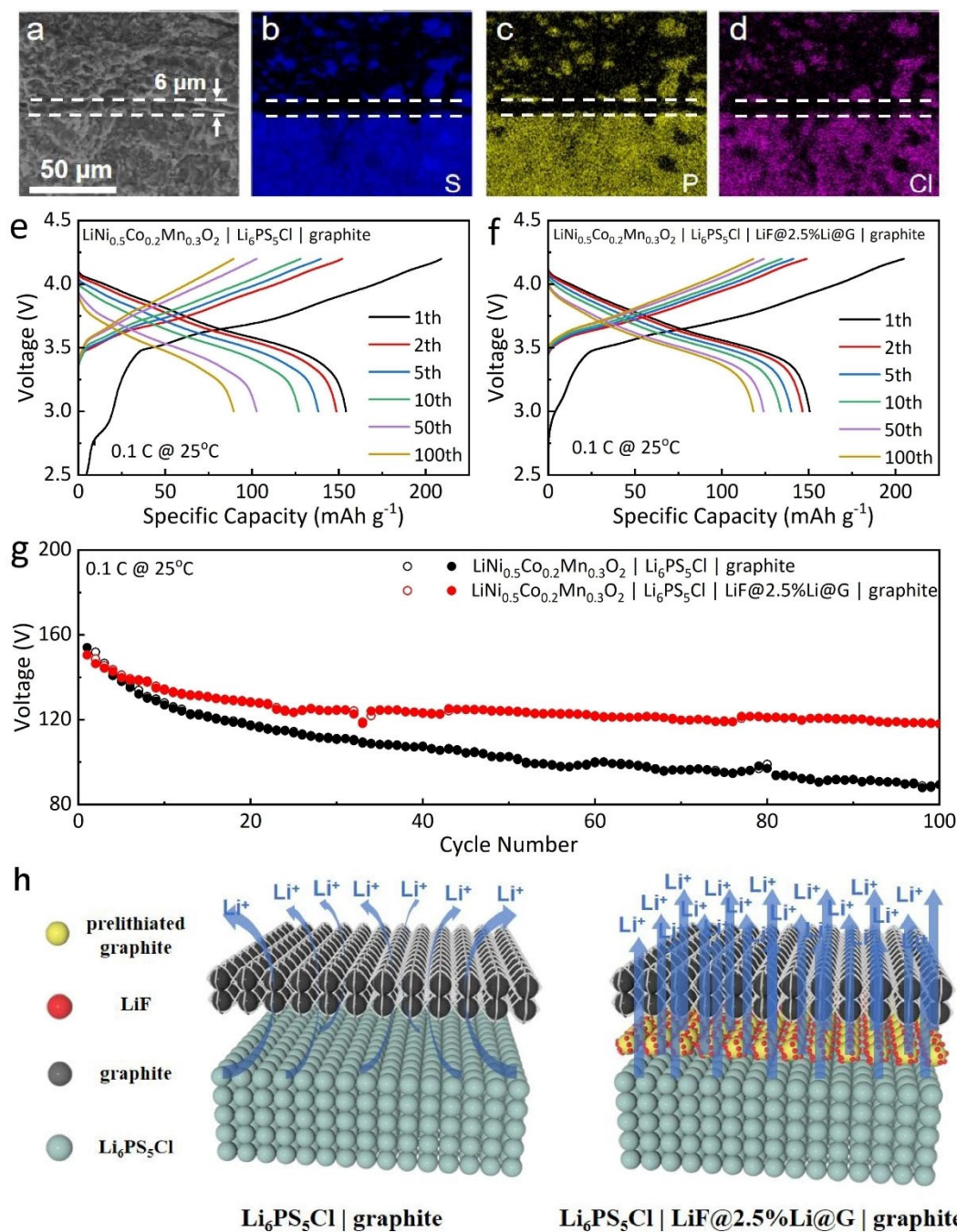
Batteries & Supercaps

Research Article
doi.org/10.1002/batt.202300488

Chemistry Europe
European Chemical
Societies Publishing

Figure 4. (a) Cross-sectional SEM image of the $LiNi_{0.5}Co_{0.2}Mn_{0.3}O_2$ | Li_6PS_5Cl | $LiF@2.5\%Li@G$ | graphite all-solid-state lithium ion battery and (b-d) the corresponding S, P, and Cl element mapping. The discharge/charge curves of (e) $LiNi_{0.5}Co_{0.2}Mn_{0.3}O_2$ | Li_6PS_5Cl | graphite and (f) $LiNi_{0.5}Co_{0.2}Mn_{0.3}O_2$ | Li_6PS_5Cl | $LiF@2.5\%Li@G$ | graphite batteries. (g) The cyclic performances of the all-solid-sate lithium ion batteries. (h) The lithium ion migration schematic diagram across the interface layer.

3. Conclusions

In this work, a LiF embedded prelithiated graphite interface layer was synthesized by spontaneous reaction of lithium with graphite and PTFE. The interface layer contains LiF, C–F bonds and prelithiated graphite, which can prevent lithium dendrite growth, facilitate uniform lithium ion migration as well as compensate the loss of active lithium in the side reactions. As a result, coupling with 6 μm-thick LiF@2.5%Li@G interface layer,

the monopolar $LiNi_{0.5}Co_{0.2}Mn_{0.3}O_2$ | Li_6PS_5Cl | $LiF@2.5\%Li@G$ | graphite all-solid-state lithium ion battery shows a high initial discharge capacity of 150.5 mAh g^{-1} with a capacity retention of 78.5% after 100 cycles at 0.1 C. In addition, the bipolar all-solid-state lithium ion batteries based on $LiNi_{0.5}Co_{0.2}Mn_{0.3}O_2$ cathode and graphite anode exhibit significantly enhanced cycling stability with capacity retention from 37% to 60.2% at 0.1 C. This work provides an effective interface strategy to improve
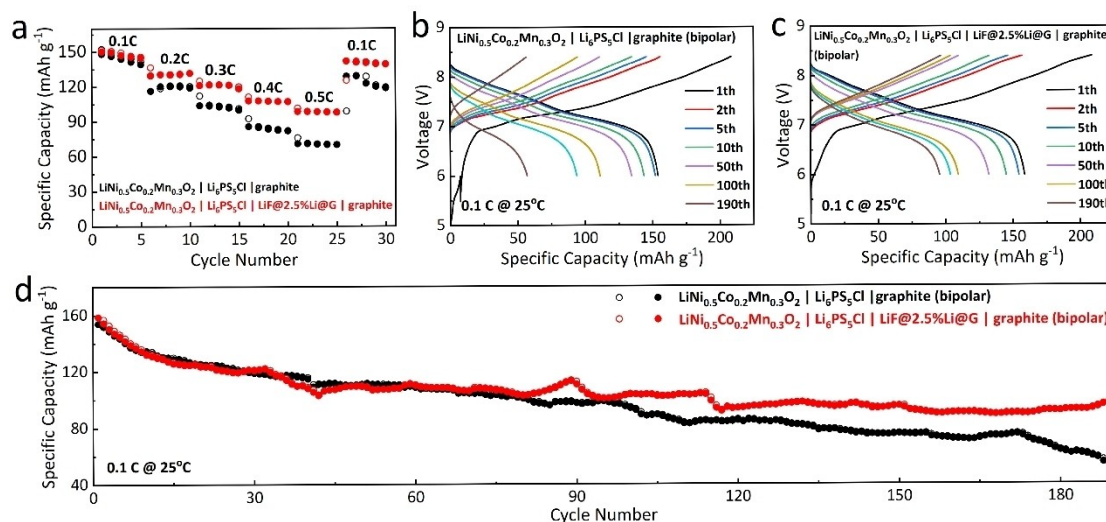
Batteries & Supercaps

Research Article
doi.org/10.1002/batt.202300488

**Chemistry
Europe**
European Chemical
Societies Publishing

Figure 5. (a) Rate performances of the all-solid-state lithium ion batteries under different current densities. (b, c) The discharge/charge profiles of the bipolar batteries. (d) The cyclic performances of the bipolar batteries.

the electrochemical performances of both monopolar and bipolar all-solid-state lithium ion batteries.

Experimental Section

Synthesis of LiF embedded prelithiated graphite

1.5 g of graphite was evenly mixed with 0.0375 g of lithium powder (2.5% weight of graphite) through a powder mixer, which was transferred to an aluminum plastic bag and pressed under 10 MPa. Then, the sample was put in an oven at 100 °C for 6 h to obtain prelithiated graphite. According to different amount lithium powder, the various degrees of prelithiated graphite can be obtained, labeled as 0.5%Li@G, 1.0%Li@G, 2.5%Li@G and 5.0% Li@G with lithium powder of 0.5 wt%, 1.0 wt%, 2.5 wt% and 5.0 wt%, respectively. For LiF embedded prelithiated graphite, 1 g of the above obtained prelithiated graphite and 0.01 g of PTFE were mixed in a powder mixer for 1 h to generate LiF embedded prelithiated graphite after standing for 6 h.

Materials characterization

X-ray diffraction analysis (XRD, D8 Advance, Bruker) with Cu K_α radiation was used to analyze the phase structures of the samples. The morphology microstructure was observed with field emission scanning electron microscopy (FESEM, S4800, Hitachi). X-ray photo-electron spectrometer (XPS) measurement was carried out using a Kratos, Axis Ultra DLD

Preparation of dry film

The graphite powder (60 wt%), Li_6PS_5Cl solid electrolyte with an ionic conductivity of 3.4 mS cm^{-1} (37 wt%) and conductive agent (2 wt%) were mixed with PTFE binder (1 wt%).[26] Then, a 90 μm-thick graphite dry film was obtained by pressing the mixed powder together between two clean rolls of a calendaring machine. The preparation process for $LiNi_{0.5}Co_{0.2}Mn_{0.3}O_2$ dry membranes is the same as described above except the ratio of $LiNi_{0.5}Co_{0.2}Mn_{0.3}O_2$, Li_6PS_5Cl, conductive agent, PTFE was set as 70:27:2:1. The thick-

ness of the $LiNi_{0.5}Co_{0.2}Mn_{0.3}O_2$ dry membrane is controlled at 75 μm. The obtained graphite and $LiNi_{0.5}Co_{0.2}Mn_{0.3}O_2$ dry films were cut into 10 mm diameter negative and positive electrodes. With the N/P ratio of 1.4, the mass loading of the graphite and $LiNi_{0.5}Co_{0.2}Mn_{0.3}O_2$ dry films are about 6.1 and 9.5 mg cm^{-2}, respectively.

Battery assembling

Laboratory-scale prototype all-solid-state lithium ion batteries with 10 mm in diameter were assembled to evaluate the electrochemical performances. All the assembling processes were conducted in a dry argon-filled glove box. First, a dense solid electrolyte layer was obtained by pressing 150 mg of Li_6PS_5Cl under 240 MPa. Then, graphite and $LiNi_{0.5}Co_{0.2}Mn_{0.3}O_2$ dry films were put in each side of the electrolyte layer, followed by pressing under 270 MPa. For the $LiNi_{0.5}Co_{0.2}Mn_{0.3}O_2 | Li_6PS_5Cl | LiF@2.5\%Li@G | graphite$ all-solid-state lithium ion battery, LiF@2.5%Li@G was put between Li_6PS_5Cl solid electrolyte layer and graphite anode layer. The obtained monopolar all-solid-state lithium ion batteries were evaluated with galvanostatic charge-discharge tests at room temperature by a standard battery testing instrument (LAND CT-2001 A, Wuhan Rambo Testing Equipment Co., Ltd.). All the tests of monopolar all-solid-state lithium ion batteries were cycled between 3.0 and 4.25 V with different current C-rates. For the assembly of bipolar all-solid-state lithium-ion batteries, the graphite dry film, LiF@2.5%Li@G, Li_6PS_5Cl solid electrolyte, and $LiNi_{0.5}Co_{0.2}Mn_{0.3}O_2$ dry film were pressed on the cathode side of the monopolar cell in turn, and fixed under 270 MPa. The bipolar battery can be regarded as two monopolar batteries in series, thus the electrochemical test voltage is set between 6.0 and 8.5 V.

4. Appendix A. Supplementary material

The following are the Supplementary material to this article:

Optical photograph of prelithiated graphite samples; Elemental mappings of graphite dry film and $LiNi_{0.5}Co_{0.2}Mn_{0.3}O_2$ dry film; The initial discharge/charge curves of graphite and $LiNi_{0.5}Co_{0.2}Mn_{0.3}O_2$ dry film; The discharge/charge curves of

Batteries & Supercaps

Research Article
doi.org/10.1002/batt.202300488

Chemistry Europe
European Chemical
Societies Publishing

batteries with graphite dry film anode and $LiNi_{0.5}Co_{0.2}Mn_{0.3}O_2$ dry film cathode under different assembly pressure; Cross-sectional SEM image of the $LiNi_{0.5}Co_{0.2}Mn_{0.3}O_2|Li_6PS_5Cl|$graphite all-solid-state lithium ion battery and the corresponding S, P, and Cl element mapping; The discharge/charge curves and cyclic performances of $LiNi_{0.5}Co_{0.2}Mn_{0.3}O_2|Li_6PS_5Cl|$graphite all-solid-state lithium ion batteries with LiF@0.5%Li@G, LiF@1%Li@G, LiF@2.5%Li@G and LiF@5%Li@G; Schematic diagram of bipolar battery structure (PDF)

Conflict of Interests

The authors declare no competing financial interest.

Data Availability Statement

The data that support the findings of this study are available from the corresponding author upon reasonable request.

[1] J. Janek, W. G. Zeier, *Nat. Energy* **2016**, *1*, 1–4.
[2] W. Fitzhugh, F. Wu, L. Ye, W. Deng, P. Qi, X. Li, *Adv. Energy Mater.* **2019**, *9*, 1900807.
[3] G. Liu, W. Weng, Z. Zhang, L. Wu, J. Yang, X. Yao, *Nano Lett.* **2020**, *20*, 6660–6665.
[4] K. J. Kim, M. Balaish, M. Wadaguchi, L. Kong, J. L. M. Rupp, *Adv. Energy Mater.* **2021**, *11*, 2002689.
[5] L. Fan, H. He, C. Nan, *Nat. Rev. Mater.* **2021**, *6*, 1003–1019.
[6] L. Wang, X. Zhang, T. Wang, Y. Yin, J. Shi, C. Wang, Y. Guo, *Adv. Energy Mater.* **2018**, *8*, 1801528.
[7] Y. G. Lee, S. Fujiki, C. Jung, N. Suzuki, N. Yashiro, R. Omoda, D. S. Ko, T. Shiratsuchi, T. Sugimoto, S. Ryu, J. H. Ku, T. Watanabe, Y. Park, Y. Aihara, D. Im, I. T. Han, *Nat. Energy* **2020**, *5*, 299–308.
[8] F. Zhao, Q. Sun, C. Yu, S. Zhang, K. Adair, S. Wang, Y. Liu, Y. Zhao, J. Liang, C. Wang, X. Li, X. Li, W. Xia, R. Li, H. Huang, L. Zhang, S. Zhao, S. Lu, X. Sun, *ACS Energy Lett.* **2020**, *5*, 1035–1043.
[9] Y. Xiao, Y. Wang, S. Bo, J. C. Kim, L. J. Miara, G. Ceder, *Nat. Rev. Mater.* **2020**, *5*, 105–126.
[10] C. Duan, Z. Cheng, W. Li, F. Li, H. Liu, J. Yang, G. Hou, P. He, H. Zhou, *Energy Environ. Sci.* **2022**, *15*, 3236–3245.
[11] X. Ji, S. Hou, P. Wang, X. He, N. Piao, J. Chen, X. Fan, C. Wang, *Adv. Mater.* **2020**, *32*, 2002741.
[12] H. Wan, S. Liu, T. Deng, J. Xu, J. Zhang, X. He, X. Ji, X. Yao, C. Wang, *ACS Energy Lett.* **2021**, *6*, 862–868.
[13] W. D. Richards, L. J. Miara, Y. Wang, J. C. Kim, G. Ceder, *Chem. Mater.* **2016**, *28*, 266–273.
[14] J. Chen, X. Fan, Q. Li, H. Yang, M. R. Khoshi, Y. Xu, S. Hwang, L. Chen, X. Ji, C. Yang, H. He, C. Wang, E. Garfunkel, D. Su, O. Borodin, C. Wang, *Nat. Energy* **2020**, *5*, 386–397.
[15] C. Liu, B. Chen, T. Zhang, J. Zhang, R. Wang, J. Zheng, Q. Mao, X. Liu, *Angew. Chem. Int. Ed.* **2023**, *135*, e2202302655.
[16] L. Shen, C. Zhao, W. Weng, M. Li, Y. Jin, Z. Zhang, X. Yao, *Adv. Mater. Interfaces* **2022**, *9*, 2200822.
[17] Y. Zhang, B. Liu, E. Hitz, W. Luo, Y. Yao, Y. Li, J. Dai, C. Chen, Y. Wang, C. Yang, H. Li, L. Hu, *Nano Res.* **2017**, *10*, 1356–1365.
[18] Q. Zhang, D. Cao, Y. Ma, A. Natan, P. Aurora, H. Zhu, *Adv. Mater.* **2019**, *31*, 1901131.
[19] S. Chen, J. Zheng, D. Mei, K. S. Han, M. H. Engelhard, W. Zhao, W. Xu, J. Liu, J. Zhang, *Adv. Mater.* **2018**, *30*, 1706102.
[20] C. Yan, Y. Yao, X. Chen, X. Cheng, X. Zhang, J. Huang, Q. Zhang, *Angew. Chem. Int. Ed.* **2018**, *57*, 14055–14059.
[21] S. Zhang, *J. Electrochem. Soc.* **2020**, *167*, 060527.
[22] H. Wang, H. An, H. Shan, L. Zhao, J. Wang, *Acta Phys. Chim. Sin.* **2021**, *37*, 2007070.
[23] S. Wang, R. Fang, Y. Li, Y. Liu, C. Xin, F. H. Richter, C. Nan, *J. Materiomics* **2021**, *7*, 209–218.
[24] F. Wang, B. Wang, J. Li, B. Wang, Y. Zhou, D. Wang, H. Liu, S. Dou, *ACS Nano* **2021**, *15*, 2197–2218.
[25] C. Sun, X. Zhang, C. Li, K. Wang, X. Sun, Y. Ma, *Energy Storage Mater.* **2020**, *32*, 497–516.
[26] Z. Zhang, L. Wu, D. Zhou, W. Weng, X. Yao, *Nano Lett.* **2021**, *21*, 5233–5239.